nature communications

Article

https://doi.org/10.1038/s41467-024-51250-8

Covalent organic framework membrane reactor for boosting catalytic performance

Received: 29 February 2024

Accepted: 2 August 2024

Published online: 09 August 2024

Check for updates

Liping Zheng[1,7], Zhengqing Zhang[2,7], Zhuozhi Lai[3], Shijie Yin[1], Weipeng Xian[3], Qing-Wei Meng[3], Zhifeng Dai[1,4] ✉, Yubing Xiong[1,4], Xiangju Meng[5], Shengqian Ma[6], Feng-Shou Xiao[3] & Qi Sun[3] ✉

Membrane reactors are known for their efficiency and superior operability compared to traditional batch processes, but their limited diversity poses challenges in meeting various reaction requirements. Herein, we leverage the molecular tunability of covalent organic frameworks (COFs) to broaden their applicability in membrane reactors. Our COF membrane demonstrates an exceptional ability to achieve complete conversion in just 0.63 s at room temperature—a benchmark in efficiency for Knoevenagel condensation. This performance significantly surpasses that of the corresponding homogeneous catalyst and COF powder by factors of 176 and 375 in turnover frequency, respectively. The enhanced concentration of reactants and the rapid removal of generated water within the membrane greatly accelerate the reaction, reducing the apparent activation energy. Consequently, this membrane reactor enables reactions that are unattainable using both COF powders and homogeneous catalysts. Considering the versatility, our findings highlight the substantial promise of COF-based membrane reactors in organic transformations.

Membrane reactors are gaining traction in the fine chemistry and pharmaceutical sectors, offering a compelling alternative to conventional batch reactors. Their unique capability to continuously remove products shifts reaction equilibria towards desired outcomes, enhancing process efficiency[1–6]. Currently, there are two predominant types of membrane reactors: those that integrate catalytically active entities within traditional polymer membranes[7–9], and those that immobilize these entities to inorganic membranes[10–13]. Despite their merits, broader adoption faces impediments. Polymer membranes often contend with restricted catalytic site accessibility and limited solvent resilience, while inorganic counterparts encounter challenges with catalytic versatility and integration synergy. As such, there is a strong need to explore new materials for constructing membrane reactors to overcome these challenges.

Covalent organic frameworks (COFs) offer a potential solution in this realm. These innovative, crystalline, porous polymers are characterized by their diverse framework topologies, open pore architectures, and customizable functionalities[14–25]. Their effectiveness in catalyzing various transformations as powders has been extensively documented[26–41]. Upon translation into membranes, COFs demonstrate potential across applications such as ion separation, energy conversion, and water purification[42–54]. The tunability of COFs enables deliberate placement of catalytic sites within robust, open membrane pore channels. Moreover, the columnar arrangement of 2D COF layers augments molecular diffusion, fortifies intermolecular interactions,

[1]Key Laboratory of Surface & Interface Science of Polymer Materials of Zhejiang Province, School of Chemistry and Chemical Engineering, Zhejiang Sci-Tech University, Hangzhou, China. [2]State Key Laboratory of Separation Membranes and Membrane Processes, School of Chemical Engineering and Technology, Tiangong University, Tianjin, China. [3]Zhejiang Provincial Key Laboratory of Advanced Chemical Engineering Manufacture Technology, College of Chemical and Biological Engineering, Zhejiang University, Hangzhou, China. [4]Longgang Institute of Zhejiang Sci-Tech University, Wenzhou, China. [5]Department of Chemistry, Zhejiang University, Hangzhou 310027, China. [6]Department of Chemistry, University of North Texas, Denton, TX, USA. [7]These authors contributed equally: Liping Zheng, Zhengqing Zhang. ✉e-mail: daizhifeng1988@163.com; sunqichs@zju.edu.cn

and ensures unimpeded access to active sites within pore channels, thus representing a significant advancement in reactor technology.

To validate the efficacy and advantages of COF-based membrane reactors, we conducted a proof-of-concept study utilizing an amine-functionalized COF membrane for the Knoevenagel condensation reaction, a key process in forming C–C bonds[55]. As a result of concentrating reactants within the membrane pores and efficiently purging water as a by-product, the reaction equilibrium favorably shifts towards desired products (Fig. 1). The outcomes of this study are striking, evincing exceptional catalytic efficiency with an unparalleled conversion rate of 100% achieved within a mere 0.63 s at room temperature. This performance substantially surpasses that of a homogeneous catalyst and COF powder, which recorded conversion rates of 71.0% and 48.5% respectively, under the conditions of 60 °C for 8 min. These results highlight the significant advantages and the promising future of COF-based membrane reactors.

Results

Membrane synthesis and characterization

Leveraging the superior catalytic properties of aminocatalysts in the Knoevenagel condensation reaction, we selected 2,5-bis(2-(dimethylamino)ethoxy)terephthalohydrazide (Bth), known for its prominent tertiary amine group, as a crucial component in synthesizing a COF membrane. The combination of Bth with 1,3,5-triformylphloroglucinol (Tp) was specifically chosen because it effectively promotes the transformation of reversible imine bonds into irreversible β-ketoenamine structures, thereby enhancing the chemical stability of the COF. To optimize operational efficiency while maintaining the organic solvent resistance and water transport efficiency of the membrane, we grow the catalytically active COF layer onto a superhydrophilic polyethersulfone (PES) surface via liquid-solid-liquid interfacial polymerization technique. The procedure entailed positioning a Tp solution in ethyl acetate and mesitylene on one side of the membrane and a Bth solution in acetic acid on the opposite side, leading to the creation of the COF-TpBth/PES membrane (Supplementary Fig. 1). Post-reaction, the membrane underwent a color shift from white to dark yellow. A water contact angle test indicated a transition from superhydrophilic to hydrophobic properties, evident in the water droplet contact angle increasing from 0° to 128°. Conversely, the contact angle for organic compounds, such as benzaldehyde, decreased from 21° on the PES to 0° (Fig. 2a and Supplementary Fig. 2). This dual organophilic and hydrophobic nature is expected to be advantageous for catalytic processes that generate water as a by-product, by facilitating the concentration of organic reactants and promote the efficient removal of H_2O.

Scanning electron microscopy (SEM) analysis unveiled distinctive surface features on the COF-TpBth/PES membrane. In contrast to the original PES surface, which featured numerous micron-sized pores, the COF-TpBth/PES membrane exhibited a more compact and smoother surface (Fig. 2b and Supplementary Fig. 3). Cross-sectional SEM images provided additional insights into the structure, revealing a COF layer thickness of approximately 200 nm (Fig. 2b, inset). Dye exclusion tests indicated that the membrane possessed diffusion channels smaller than methyl blue (2.3 nm), affirming a defect-free structure in the COF-TpBth/PES membrane (Supplementary Fig. 4). To ascertain the successful creation of the β-ketoenamine COF structure in the COF-TpBth membrane, multiple analytical methods were employed. For characterization purposes, the PES substrate was dissolved in dimethyl sulfoxide (DMSO). Fourier-transform infrared spectroscopy (FT-IR) results were particularly informative, showcasing the disappearance of characteristic aldehyde group signals from Tp and $-NH_2$ signals from Bth. Additionally, new signals corresponding to amide C = O and C = C vibrations emerged, strongly suggesting the formation of the β-ketoenamine COF (Supplementary Fig. 5)[56]. Solid-state ^{13}C nuclear magnetic resonance (^{13}C NMR) spectroscopy further substantiated this conclusion by displaying characteristic C = O signals at 190.0 ppm (Supplementary Fig. 6). Powder X-ray diffraction (PXRD) patterns demonstrated excellent crystallinity, with diffraction peaks aligning with the eclipse AA stacking structures (Fig. 2c). N_2 sorption isotherms revealed a Brunauer–Emmett–Teller (BET) surface area of 459 $m^2\ g^{-1}$ for COF-TpBth. Pore size distribution analysis indicated an average pore size of about 2.0 nm, consistent with the proposed structures (Supplementary Fig. 7). To assess the inherent basic strength of the COF-TpBth/PES membrane, we employed an in-situ probe molecule adsorption technique in conjunction with FT-IR spectroscopy (Supplementary Fig. 8). Deuterated chloroform ($CDCl_3$), chosen for its mild acidity, was selected as the probe. Following the adsorption of $CDCl_3$, FT-IR analysis revealed a broad absorption band between 2180 − 2290 cm^{-1}, indicating the stretching vibrations (ν_{CD}) of the C − D bond in $CDCl_3$. According to the equation: $\log \Delta\upsilon_{CD} = 0.0066PA - 4.36$, where $\Delta\upsilon_{CD}$ represents the shift in ν_{CD} (cm^{-1}), and PA is the proton affinity (kJ mol^{-1}), revealing that COF-TpBth exhibits moderate basicity[57].

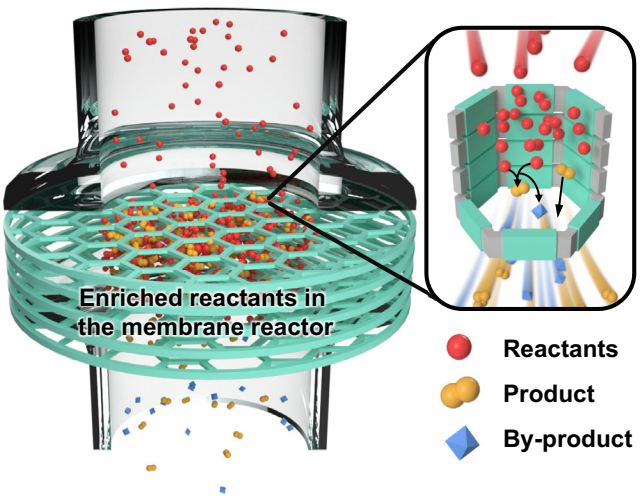

Fig. 1 | Conceptual diagram illustrating the deployment of a membrane reactor based on COFs for highly efficient catalysis. The membrane facilitates the enrichment of reactants and rapid removal of products during the catalytic process.

Catalytic efficiency evaluation

To assess the efficacy of COF-TpBth/PES as a membrane reactor, we selected the Knoevenagel condensation of benzaldehyde with malononitrile, resulting in the formation of benzalmalononitrite, as a representative model reaction. The catalytic process occurred within a specially designed dead-end membrane system (Fig. 3a). The experimental procedure involved loading the feed chamber with a 0.5 mL ethanol solution containing 0.5 M benzaldehyde and 0.55 M malononitrile (ethanol was identified as the optimal solvent through solvent screening experiments, Supplementary Fig. 9). A constant vacuum suction was applied to facilitate the permeation of this mixture through the membrane, propelling the reactants to traverse the membrane and enhancing the interaction with the catalytic sites within the pore channels of the membrane reactor. The catalytic reaction initiated upon the contact of the reactants with the active sites of the COF reactor during the transmembrane process. Simultaneously, the filtrate was collected in a flask, and the yield of the membrane catalysis was determined using ^1H NMR spectroscopy. The volumetric flow rate of the reaction mixture remained constant, as evidenced by a linear flow volume-time relationship (Supplementary Fig. 10). Furthermore, the membrane flux exhibited an almost linear increase as the vacuum suction increased up to 0.8 bar (Supplementary Fig. 11).

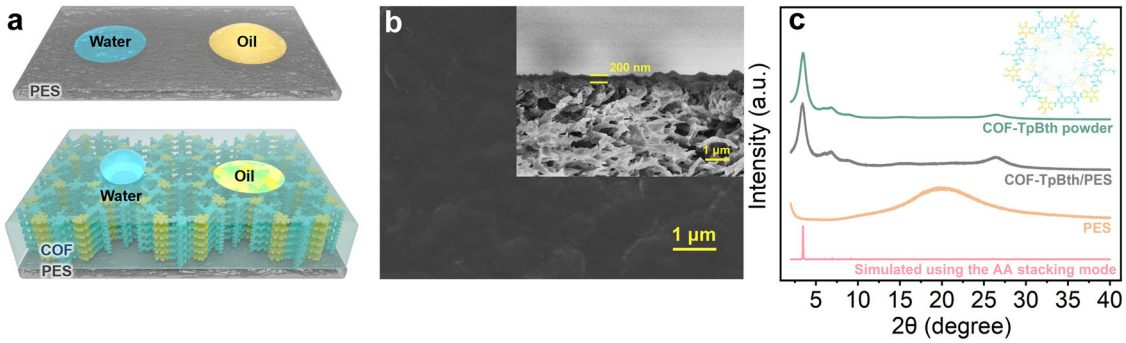

Fig. 2 | Membrane characterization. a Depiction of the COF-TpBth/PES composite membrane structure and the wettability comparison between the PES substrate and the COF-TpBth/PES membrane. **b** SEM images of the COF-TpBth/PES membrane with an inset showing the cross-sectional view. **c** PXRD patterns, with an inset displaying the chemical structure of COF-TpBth.

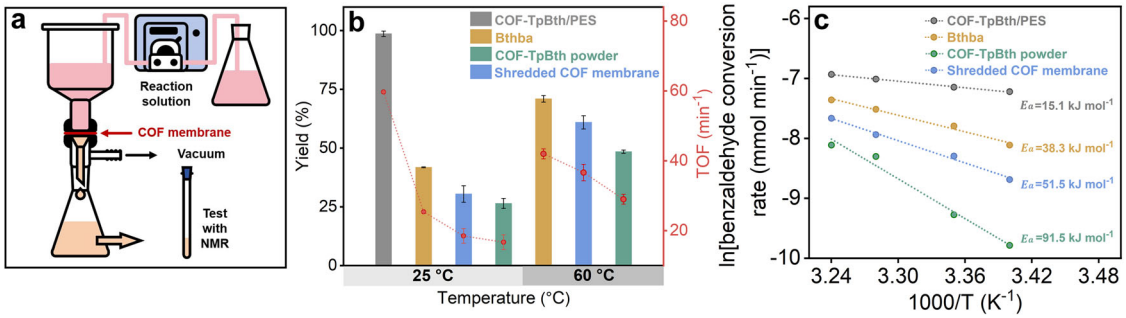

Fig. 3 | Setup for membrane reactions and evaluation of catalytic performance. a Schematic representation of the membrane catalysis experimental setup. **b** Comparative analysis of catalytic efficiency among the COF-TpBth/PES membrane, a shredded COF membrane, the corresponding COF powder, and a homogeneous catalyst (Bthba). The grey areas on the x-axis indicate the reaction temperatures corresponding to the catalytic data obtained above. The error bars represent the standard deviation of three independent measurements of the various membranes. **c** Arrhenius plots along with the corresponding apparent activation energies.

The efficacy of the membrane reactor was benchmarked against three distinct catalytic systems: a shredded COF membrane, COF powder, and a homogeneous catalyst (Bthba) derived from Bth and benzaldehyde, and all the measurements were replicated with three independent experiments. Batch reactions for these catalytic systems, with the exception of the membrane reactor, were carried out using reaction volumes derived from the permeance of the membrane reactor, maintaining identical temperature conditions and stirring. The membrane reactor exhibited exceptional performance, achieving complete conversion of benzaldehyde under a vacuum suction of 0.05 bar, maintaining in a stable turnover frequency (TOF) of $60 \pm 0.23\ min^{-1}$ over a period of 8 min. This performance greatly surpassed that of the batch reactions, where the initial turnover frequencies for the shredded membrane, COF powder, and homogeneous catalyst were 18, 16, and $25\ min^{-1}$, respectively, under similar conditions. Notably, the contact time between the solution and the membrane, calculated based on the volumes of the reaction solution and the COF active layer, was only 0.63 s to achieve 100% conversion (see details in the Supplementary Methods). In contrast, at 60 °C over an 8-minute period, the shredded COF membrane, the COF powder, and the Bthba catalyst reached conversion rates of 61.0%, 48.5%, and 71.0%, respectively (Fig. 3b).

To further elucidate the experimental observations, we undertook additional experiments. We began by calculating the activation energies (E_a) for the condensation of benzaldehyde with malononitrile. This involved analyzing Arrhenius plots, which correlate product yield with reaction temperature, as shown in Supplementary Fig. 12. The results revealed E_a values of 15.1 kJ mol^{-1} for the membrane reactor, 91.5 kJ mol^{-1} for the COF powder, 51.5 kJ mol^{-1} for the shredded COF membrane, and 38.3 kJ mol^{-1} for the homogeneous Bthba catalyst (Fig. 3c). The relatively low E_a for the membrane reactor suggests its superior efficiency in activating reactants, thereby enhancing the rate of the Knoevenagel condensation reaction. The disparity in catalytic performance among these systems, despite similar active sites, is primarily attributed to two factors. First, the synergy between the hydrophobic COF layer and the superhydrophilic PES substrate in the membrane reactor. This unique combination boosts reactant concentration while simultaneously repelling water (a by-product), continuously shifting the reaction equilibrium towards product formation, leading to higher single-pass conversion. This is also evidenced by the superior performance of the shredded COF membrane compared to the COF powder. Second, the pressure-driven transit of reactant molecules through the narrow COF pore channels, which likely aligns them in an orderly manner and enhances their interaction with active sites, thereby facilitating the reaction and reducing the activation energy[58–60].

Investigation of the influence of reactant concentration on the reaction

Subsequently, experiments were carried out over a range of initial reactant concentrations from 0.1 to 0.9 M. In Fig. 4a, the rate of benzaldehyde conversion and TOF are plotted against the initial benzaldehyde concentration (the concentration of malononitrile is 1.1 times that of benzaldehyde). For concentrations between 0.1 to 0.5 M, both plots exhibit linearity. However, at 0.5 M, the conversion rate peaks and then decreases with further concentration increases, while the TOF continues to rise as reactant concentration increases. This trend suggests a strong dependency of the reaction rate on reactant

https://doi.org/10.1038/s41467-024-51250-8

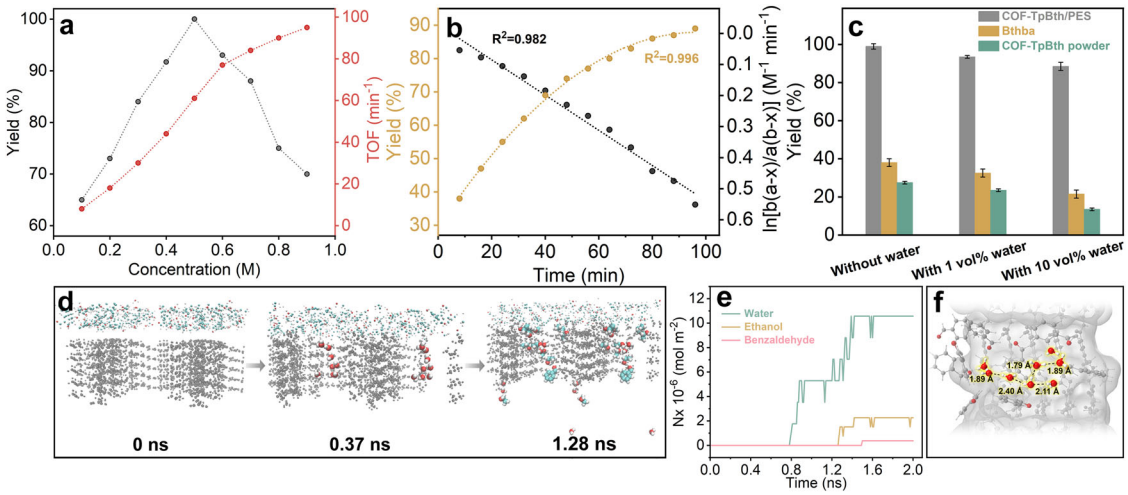

Fig. 4 | Investigation of reaction order and transport kinetics across the membrane for various molecules. a Assessment the impact of reactant concentration on the performance of COF-TpBth/PES. The grey areas on the x-axis indicate the reactant concentrations and vacuum suction applied in relation to the catalytic data obtained above. **b** Time-dependent variation of product yield in Knoevenagel condensation catalyzed by Bthba at room temperature. The accompanying empirical equation is derived from linear fitting. **c** Evaluating the influence of water on reaction efficiency across different catalytic systems. **d** Snapshots illustrating the dynamic behavior of benzaldehyde, ethanol, and water within COF-TpBth nanochannels at specific time points (0, 0.37, and 1.28 ns). The diffusion rates follow the order: H_2O > ethanol > benzaldehyde (red, O; white, H; cyan, C; grey, COF-TpBth). Some molecules in the pore channel are depicted as dots for clarity. **e** Statistical analysis of transmembrane molecule permeation across the COF membrane. (f) A magnified view highlighting a pore channel of the COF membrane reactor filled with a hydrogen-bonded water wire. Hydrogen-bonding interactions among the H_2O molecules are observable. These interactions, combined with the hydrophobic environment created by surrounding benzaldehyde molecules, are expected to align the H_2O molecules linearly along the pore channels.

concentration. To quantitatively analyze the reaction order, the homogeneous Bthba catalytic system was studied. The time-dependent product yield curve in Fig. 4b shows a linear relationship between time (t) and the concentration expression $\ln[(b(a-x))/(a(b-x))]$. In this expression, x represents the product (benzalmalononitrite) concentration, t is the reaction time, and a and b are the initial concentrations of malononitrile and benzaldehyde, respectively. The correlation coefficient of this relationship is notably high at 0.982, suggesting that the reaction follows a pseudo-second-order kinetic model[61,62]. To further investigate the individual effects of benzaldehyde and malononitrile concentrations on the reaction, their concentrations were varied separately in a series of experiments. It was observed that the influence of these two reactants on the reaction kinetics was nearly identical, suggesting a comparable impact from both benzaldehyde and malononitrile (Supplementary Fig. 13). Both the COF powder and membranes used in batch reactions displayed similar rate constant terms for benzaldehyde and malononitrile as observed with the homogeneous catalyst Bthba (Supplementary Figs. 14 and 15). These findings underscore the significant role that reactant concentration plays in dictating the reaction rate; as concentrations decrease during the reaction, the reaction rate also tends to diminish.

A comprehensive examination of the influence of reactant concentration on the membrane reactor, COF powder, and the homogeneous Bthba catalytic system revealed that the batch reaction system was more sensitive to decreases in reactant concentration. For example, a reduction in concentration from 0.5 M to 0.1 M resulted in a 35% decrease in conversion rate in the membrane reactor, falling from 100% to 65%. In contrast, the conversions of benzaldehyde in the homogeneous and COF powder systems dropped by 45% and 41% respectively, indicating that reactants can be effectively enriched during catalysis (Supplementary Fig. 16).

Investigation of the influence of H_2O on the reaction

We observed a significant decline in the growth rate once specific conversion thresholds were reached: 80% for COF powder and 90% for the homogeneous Bthba catalyst. Specifically, the conversion of benzaldehyde in the COF powder reached 78% after 80 min, then increased to 84% and 91% after 648 min and 1440 min, respectively (Supplementary Fig. 17). Further extending the reaction time to 48 h only minimally enhanced the yield to 92%. Consequently, the overall TOF values for the homogeneous catalyst and the COF powder were calculated to be 0.34 min^{-1} (at 100% conversion) and 0.16 min^{-1} (at 92% conversion), respectively. These values are 176 and 375 times smaller than that of the corresponding membrane reactor. This pattern led us to hypothesize that the accumulation of by-product H_2O might be inhibiting the reaction. In the membrane-catalyzed process, produced H_2O molecules are instantly separated from the phase, a process enhanced by the hydrophobic and superhydrophilic structure of the composite membrane. However, in batch reactions, all the generated H_2O remains in the solution. As the reaction continues, the concentration of reactants decreases, while that of by-product H_2O increases, making the reaction increasingly difficult. To validate this presumption, we evaluated the effect of H_2O on catalytic efficiency. The results showed that introducing 10 vol% H_2O into the reaction mixture decreased the efficiency of the membrane reactor by roughly 9%, while the efficiencies of the COF powder and homogeneous catalyst systems dipped by 52% and 42% respectively. This finding reinforces the assumption that by-product water exerts a negative influence on the reaction efficiency (Fig. 4c).

Molecular dynamics (MD) simulation

To assess the effectiveness of the COF membrane reactor in concentrating reactants and excluding water at a molecular level, MD simulations were performed (Supplementary Fig. 18). These simulations analyzed the diffusion dynamics of benzaldehyde, ethanol, and water through the membrane. The findings showed a consistent decrease in the transmembrane transport rates for these molecules, with water having the highest rate, followed by ethanol, and benzaldehyde the slowest (Fig. 4d and Supplementary Movie 1). This outcome was further corroborated by statistical analysis of molecule permeation across the COF membrane (Fig. 4e). Specifically, MD

simulation snapshots recorded the penetration times of the first water, ethanol, and benzaldehyde molecules through the membrane as 0.09 ns, 1.28 ns, and 1.52 ns, respectively (Supplementary Fig. 19). A detailed analysis was conducted on the transmembrane behavior of these molecules through the channels of COF-TpBth membranes. It was observed that benzaldehyde molecules oscillated within the pore channels, while water molecules quickly passed through. In the transport process of water molecules, an intermittent water wire formed, which, surrounded by hydrophobic benzaldehyde molecules, arranged the water molecules into single-file, one-dimensional configurations, enhancing their movement along the pore channel (Fig. 4f)[63,64]. The oscillations of the side chains on the COF pore walls contributed to the transient nature of the water wire. The rapid diffusion of water molecules led to their effective exclusion from the reactor. Meanwhile, the faster diffusion of ethanol, serving as the solvent, compared to the reactant benzaldehyde, resulted in a higher concentration of the reactant within the membrane reactor. This differential behavior significantly enhanced the efficiency of the COF membrane reactor by maintaining high reactant concentrations and rapidly excluding water, thus potentially reducing its inhibitory impact on the reaction process. Furthermore, through detailed MD simulations analyzing the transmembrane transport behavior of benzaldehyde molecules, we indeed observed that upon entering the confined pore channels, the benzaldehyde molecules form intermolecular hydrogen bonds, which orient them within the channels. Additionally, these molecules also engage in hydrogen bonding with the COF backbone (Supplementary Fig. 20).

The general advantage of transforming COF powder into a membrane reactor

To highlight the unique capability of promoting reactions through the transformation of COF powder into a membrane reactor, we developed an alternative membrane reactor by condensing Tp with terephthalohydrazide (Tph, Supplementary Fig. 21). This fabricated reactor (COF-TpTph/PES) revealed weakly basic sites of amide nitrogen as demonstrated by $CDCl_3$ adsorption experiments (Supplementary Fig. 22). Under operation conditions of 0.5 M reactant concentration and 0.05 bar pressure, the reactor accomplished a 23% yield in benzaldehyde conversion. Notably, in direct comparison, the corresponding COF powder and homogeneous catalytic systems achieved conversion rates of only 4% and 7% respectively. Even more striking, when the reactant concentration was decreased to 0.1 M and the vacuum suction increased to 0.1 bar, the membrane reactor was still able to maintain an 8% benzaldehyde conversion rate, while no conversion was discernible in either the COF powder or homogeneous systems (Fig. 5a). These results underscore the ability of the COF membrane to reduce the activation energy of the reaction, likely due to the unique packing of reactants within the confined nanochannels of the membrane reactor, a process augmented by vacuum suction.

Long-term efficiency evaluation

To further evaluate the efficiency of the COF-TpBth/PES membrane reactor, a 48-hour continuous operation test was performed. Under optimized conditions consisting of a 0.5 M concentration of benzaldehyde and a pressure of 0.05 bar, the membrane reactor consistently achieved a conversion rate exceeding 95% for benzaldehyde, demonstrating its stable and efficacious performance over the prolonged period. Contrastingly, the homogeneous catalytic system and the COF-TpBth powder, under identical conditions, achieved lower conversion rates of 85% and 49% respectively. Moreover, to achieve a benzaldehyde conversion rate analogous to that of the membrane reactor, the homogeneous Bthba catalytic system and COF-TpBth powder necessitated substantially longer durations of 98 h and an extensive 210 h, respectively (Supplementary Fig. 23). Importantly, the integrity and the crystallinity of the membrane were maintained after catalysis (Supplementary Figs. 24 and 25).

Subsequent investigations focused on the impact of pressure on the catalytic efficiency of the membrane reactor. A key finding was the observed enhancement in the TOF of benzaldehyde with increasing pressure (Fig. 5b). This improvement in performance is likely due to the increased pressure, which enlarges the diffusion rates of the reactants, solvent, and water, thereby concentrating the reactants more effectively. As a result, a significant increase in TOF was observed, rising from 60 to 185.2 min^{-1} as the vacuum suction intensified from 0.05 to 0.8 bar, establishing a benchmark in the field of Knoevenagel condensation (Fig. 5c and Supplementary Tables 1–3).

Exploration of reaction scope

To evaluate the adaptability of our membrane reactor across diverse substrates, we broadened our investigation to encompass a variety of substituted benzaldehydes undergoing Knoevenagel condensation with malononitrile. This exploration allowed us to further accentuate the advantages of the membrane reactor by comparing its performance with a homogeneous catalytic system. To optimize the reaction rate, we maintained a constant pressure of 0.7 bar and utilized aldehyde and malononitrile at concentrations of 0.5 M and 0.55 M, respectively. Our findings revealed that the membrane reactor efficiently catalyzes the Knoevenagel condensation of various aldehydes. We observed that electron-withdrawing groups on the benzene ring, such as in 2-fluorobenzaldehyde, afforded a greater efficiency, achieving a TOF of up to 183 min^{-1}. Conversely, electron-donating groups tended to reduce the reaction rate, particularly when positioned at the para position of the benzene ring, as in 4-methoxybenzaldehyde, though the TOF remained impressively high. Significantly, the membrane reactor consistently outperformed the homogeneous system, with TOF values ranging from 1.45 to 2.86 times higher. It is important to note that these TOF values were determined within the initial 8 minutes. As the reactant concentration decreased and water molecules were generated, the reaction rate of the batch

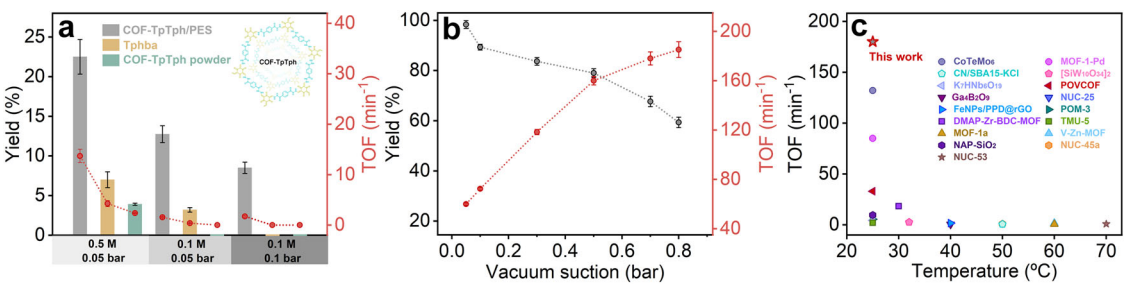

Fig. 5 | Comparative catalytic performance across diverse catalytic systems. **a** Comparative analysis of catalytic efficiency among the COF-TpTph/PES membrane, the corresponding COF powder, and a homogeneous catalyst (Tphba) derived from Tph and benzaldehyde. **b** Examination of the influence of vacuum suction magnitude on the catalytic efficiency of the COF-TpBth/PES membrane reactor. **c** Comparison between the COF-TpBth/PES membrane reactor and previously reported catalytic systems (see details in Supplementary Table 1).

https://doi.org/10.1038/s41467-024-51250-8

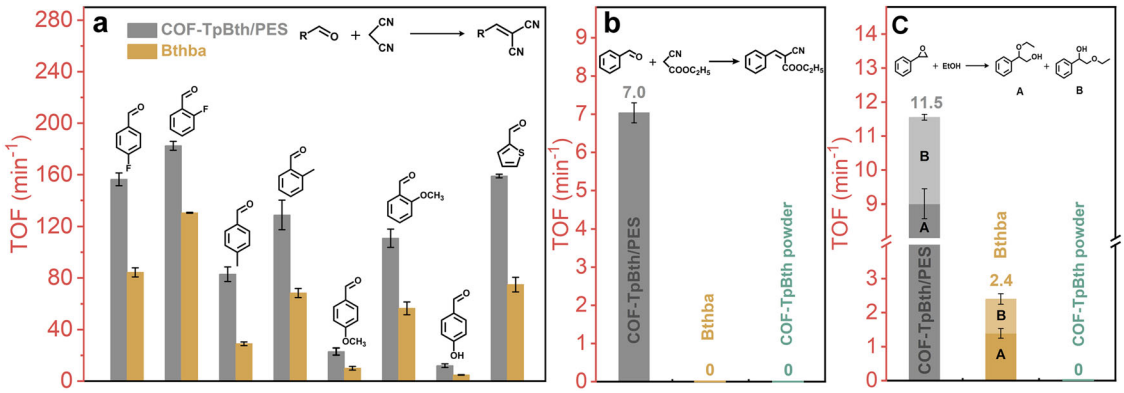

Fig. 6 | Exploration of reaction scope. a Comparative analysis between the COF-TpBth/PES membrane reactor and the homogeneous Bthba catalyst. **b** Catalytic efficiency in the condensation of benzaldehyde and ethyl cyanoacetate across different catalytic systems. **c** Catalytic efficiency in the ring-opening reaction between styrene oxide and ethanol across different catalytic systems.

reaction decreased significantly. Consequently, there is expected to be a more pronounced difference in TOF values between the batch reaction and the membrane catalysis when the reactions achieve full conversion. This disparity inversely correlated with the reaction efficiency: lower efficiencies in the homogeneous system corresponded to larger improvements in the membrane reactor. This suggests that the membrane reactor can effectively lower the apparent activation energy, facilitating the reaction process. Moreover, the membrane reactor also exhibited excellent catalytic performance in the Knoevenagel condensation of heterocyclic aldehyde. In this case, the aldehyde TOF achieved was 159 min^{-1}, which is 2.12 times higher than that of the corresponding homogeneous system (Fig. 6a). This underscores the broad applicability and efficiency of membrane reactor in various organic transformations.

To further demonstrate the efficacy of the COF-TpBth/PES membrane reactor, a comparative analysis was conducted on its performance in the condensation of benzaldehyde with ethyl cyanoacetate. The COF-TpBth/PES membrane reactor achieved a TOF of 7.0 min^{-1}, whereas the homogeneous catalyst Bthba and the COF powder catalyst did not produce any detectable products (Fig. 6b). Additionally, the membrane reactor proved effective in the ring-opening reaction between styrene oxide and ethanol, delivering a TOF of 11.5 min^{-1}. Under identical conditions, Bthta achieved only a TOF of 2.4 min^{-1}, and the COF powder catalyst yielded no detectable product (Fig. 6c). These results not only highlight the advantages of the membrane reactor in lowering the activation energy and enhancing the overall efficiency of the reaction but also suggest that the COF membrane could be applicable to a broader range of base-catalyzed reactions.

Discussion

In summary, this study underscores the significant advantages of employing COFs as membrane reactors, especially when compared to their homogeneous equivalents and COF powders in the context of Knoevenagel condensation. The superiority of COF membrane reactors is demonstrated in several key aspects. Firstly, the COF membrane reactor achieves a remarkable 100% conversion in just 0.63 s at room temperature, a remarkable feat compared to the days required by the homogeneous catalyst and COF powder under the same conditions. Secondly, the membrane reactor significantly reduces the activation energy required for the reactions, thereby enhancing the catalytic process, thus fostering the catalytic transformation while both the homogeneous counterpart and the COF powder cannot activate such a reaction. To our knowledge, this study represents the initial exploration into using a COF-based membrane reactor. Considering the wide array of COF materials available, the potential applications of COF-based membrane reactors are poised to open up avenues for improved catalysis in the future.

Methods

Materials

Commercially available reagents were procured in high purity and utilized without additional purification. The synthetic procedures for other monomers employed in the COF membrane synthesis are outlined in the Material Synthesis section, with their purity confirmed through NMR analysis. 0.2 μm Supor 200 PES Membrane Disc Filter was sourced from Pall Corporation (New York, NY, USA).

Material synthesis

Diethyl 2,5-bis(2-(dimethylamino)ethoxy)terephthalate. In a reaction flask containing diethyl 2,5-dihydroxyterephthalate (4 g, 15.7 mmol), Cs_2CO_3 (21.6 g, 66 mmol), and CH_3CN (100 mL), 2-dimethylaminoethyl chloride hydrochloride (4.8 g, 33.3 mmol) was added incrementally. The resulting mixture was heated at 110 °C for 24 hours. After evaporation of CH_3CN, the brownish residue was dissolved in H_2O and extracted with ethyl acetate (EtOAc). The combined organic phase was acidified with HCl (3 M, 3 ×30 mL), and the resulting aqueous phase was washed with diethyl ether (3 ×30 mL), alkalized with K_2CO_3, and further extracted with EtOAc. The organic layer was dried over magnesium sulfate. The resultant title product was obtained as a brown liquid after removing EtOAc (3.86 g, 9.8 mmol, 62%). ^{1}H NMR (500 MHz, $CDCl_3$): δ = 7.40 (s, 2H), 4.36 (q, 4H), 4.11 (t, 4H), 2.75 (t, 4H,), 2.35 (s, 12H), 1.38 (t, 6H) ppm.

2,5-Bis(2-(dimethylamino)ethoxy)terephthalohydrazide (Bth). Diethyl 2,5-bis(2-(dimethylamino)ethoxy)terephthalate (2.0 g, 5.0 mmol) was added to a mixture of toluene (40 mL) and ethanol (40 mL). Hydrazine hydrate (6.5 mL) was then added dropwise, and the resulting mixture was refluxed overnight at 110 °C (Supplementary Fig. 26a). After cooling, the solution was evaporated under vacuum, resulting in the formation of the title compound Bth as a yellow solid (1.62 g, 4.4 mmol, 88% yield). ^{1}H NMR (500 MHz, $CDCl_3$): δ = 10.52 (s, 2H), 7.76 (s, 2H), 4.23 (t, 4H), 4.17 (bs, 4H), 2.70 (t, 4H), 2.33 (s, 12H) ppm.

Terephthalohydrazide (Tph). Diethyl terephthalate (1.5 g, 6.8 mmol) was added to ethanol (40 mL). Hydrazine hydrate (6.5 mL) was introduced dropwise, and the resulting mixture was refluxed overnight at 110 °C (Supplementary Fig. 26b). After cooling, the solution was evaporated under vacuum, resulting in the formation of the title compound Tph as a white solid (1.19 g, 6.1 mmol, 90% yield). ^{1}H NMR (500 MHz, d_6-DMSO): δ = 9.89 (s, 2H), 7.83 (s, 4H), 4.55 (s, 4H) ppm.

Bthba. Bth (184.2 mg, 0.5 mmol), benzaldehyde (106.2 mg, 1.0 mmol), and ethanol (10 mL) were added to a round-bottom flask. The resulting mixture was stirred for 12 hours at 50 °C. Following this, the solution was evaporated under vacuum (Supplementary Fig. 26c). The resulting solid was washed with diethyl ether and vacuum-dried, yielding the final product as a white solid (223.3 mg, 82%). ^{1}H NMR (500 MHz, $CDCl_3$): δ = 11.95 (s, 2H), 8.30 (s, 2H), 8.01 (s, 2H), 7.84-7.79 (m, 4H), 7.47-7.42 (m, 6H), 4.35 (t, 4H), 2.83 (t, 4H), 2.37 (s, 12H) ppm.

Tphba. Tph (97.4 mg, 0.5 mmol), benzaldehyde (106.2 mg, 1.0 mmol), and ethanol (10 mL) were added to a round-bottom flask. The resulting mixture was stirred for 12 hours at 50 °C. Following this, the solution was evaporated under vacuum (Supplementary Fig. 26d). The resulting solid was washed with diethyl ether and vacuum-dried, yielding the final product as a white solid (166.6 mg, 90%). ^{1}H NMR (500 MHz, d_6-DMSO): δ = 11.99 (s, 2H), 8.46 (s, 2H), 8.04 (s, 4H), 7.73 (d, 4H), 7.47-7.42 (m, 6H) ppm.

COF-TpBth/PES. The active layers of the COF were synthesized through interface polymerization on the surface of a PES ultrafiltration membrane. The PES support was positioned vertically in the center of a custom-made diffusion cell, with each compartment having a volume of 7 cm^3. An acetic acid aqueous solution (1 M, 7 mL) containing Bth (57.8 mg, 0.15 mmol), and a solution of Tp (22.0 mg, 0.105 mmol) in a mixture of ethyl acetate (EtOAc) and mesitylene (V/V = 1/9, 7 mL) were separately introduced into the two sides of the diffusion cell. The reaction mixture was maintained at 35 °C for 3 days. The resulting membrane, designated as COF-TpBth/PES, was rinsed with methanol to eliminate any residual monomers and the catalyst (Supplementary Fig. 27a). Given the challenge of accurately measuring such a thin COF active layer that is integrated with PES, we employed a rigorous method for calculating the mass of the COF membrane, which was determined to be approximately 0.035 mg. This calculation took into account the effective surface area of the COF-TpBth/PES membrane using the formula πr^2, where r, the radius of the effective membrane area, is 0.75 cm (according to the effective surface during catalysis). The thickness of the membrane, as determined by the cross-sectional SEM images, is 200 nm. Additionally, we utilized zeo++ software to calculate the density and accessible volume of the COF-TpBth material, found to be 0.889507 g cm^{-3} and 0.629337 cm^3 g^{-1}, respectively. Our N_2 sorption isotherms indicated a pore volume of 0.338977 cm^3 g^{-1} for the synthesized COF-TpBth, which is lower than the theoretical value. Given that the densities of COFs are typically less than 1 g cm^{-3}, we assumed a density of 1 g cm^{-3} for the COF-TpBth active layer to facilitate a balanced comparison. This assumption results in the computed mass of the COF active layer on PES being 0.035 mg. Moreover, based on the COF's structure, the membrane's content of active sites is approximately 0.15 μmol.

COF-TpTph/PES. The active layers of the COF were synthesized through interface polymerization on the surface of a PES ultrafiltration membrane. The PES support was positioned vertically in the center of a custom-made diffusion cell, with each compartment having a volume of 7 cm^3. An acetic acid aqueous solution (1 M, 7 mL) containing Tph (29.1 mg, 0.15 mmol), and a solution of Tp (22.0 mg, 0.105 mmol) in a mixture of ethyl acetate (EtOAc) and mesitylene (V/V = 1/9, 7 mL) were separately introduced into the two sides of the diffusion cell. The reaction mixture was maintained at 35 °C for 3 days. The resulting membrane, designated as COF-TpTph/PES, was rinsed with methanol to eliminate any residual monomers and the catalyst (Supplementary Fig. 27b).

COF-TpBth powder. A 10 mL of Schlenk tube was loaded with Tp (22.0 mg, 0.105 mmol), Bth (57.8 mg, 0.15 mmol), ethanol (1.02 mL), mesitylene (0.18 mL), and 6 M aqueous acetic acid (0.1 mL). After a brief sonication, the tube was then placed in an oven at 85 °C for 3 days. The resulting precipitate was filtered, thoroughly washed through Soxhlet extractions with methanol and acetone for 2 days, and air-dried at ambient temperature for 24 hours. The resulting COF-TpBth powder was isolated as a brown powder.

Characterization

Scanning electron microscopy (SEM) was conducted using a Hitachi SU 8000 instrument. FTIR spectra were recorded using a Nicolet Impact 410 FTIR spectrometer. Gas adsorption isotherms were obtained with a surface area analyzer ASAP 2020, and N_2 sorption isotherms were measured at 77 K using a liquid N_2 bath. PXRD data were collected on a Bruker AXS D8 Advance A25 powder X-ray diffractometer (40 kV, 40 mA) with Cu Kα (λ = 1.5406 Å) radiation. Dye concentrations were determined using Thermo Scientific™ UV-Vis spectrophotometers. Contact angles of water were measured using a contact angle measuring system SL200KB (USA KNO Industry Co.), equipped with a CCD camera. ^{13}C cross-polarization magic-angle spinning (CP-MAS) was recorded on a Bruker Avance Neo 600WB spectrometer at a resonance frequency of 150.94 MHz. ^{1}H NMR spectra were recorded on a Bruker Avance III 500 (500 MHz) spectrometer. $CDCl_3$-IR measurements were carried out in a Bruker VERTEX 80 v spectrometer, between 4000 and 400 cm^{-1} with a resolution of 4 cm^{-1}.

Catalytic performance evaluation

Membrane catalysis in the condensation of benzaldehyde and malononitrile. The catalytic process took place in a home-made dead-end membrane system at room temperature (25 °C) with a feed chamber diameter of 1.5 cm. The entire membrane had a diameter of 2.5 cm, with the central 1.5-cm area being the primary region involved in the reaction, containing 0.15 μmol of tertiary amine sites within the COF active layer. Subsequently, a 0.5 mL ethanol solution containing malononitrile (0.55 M) and benzaldehyde (0.5 M) was introduced into the feed chamber. To facilitate the permeation of the ethanol solution through the membrane and promote the transit of reactants across the membrane, a constant vacuum suction was applied. This enhanced interaction with the catalytic sites located within the pore channels of the membrane reactor. The reactants underwent reactions within the pore channels, and the resulting products exited along with the ethanol solvent. The filtrate, containing the reaction products, was collected in a flask, and the yield of the membrane catalysis was determined using ^{1}H NMR spectroscopy.

Batch reactions in the condensation of benzaldehyde and malononitrile. The volumes of the reaction solutions for batch reactions were determined based on the flux through the membrane. For example, in the COF-TpBth/PES membrane reactor operating at a temperature of 25 °C and under a vacuum suction of 0.05 bar, 0.15 mL of solution passed through within 8 minutes. The quantities of COF powders and homogeneous catalysts used were calculated based on the mass of the COF active layers. To aid in the weighing process, the batch reactions were scaled up by a factor of 100. The reaction mixture consisted of an ethanol solution with benzaldehyde (0.5 M, 7.5 mmol, 795.9 mg) and malononitrile (0.55 M, 8.25 mmol, 495.5 mg), totaling 15 mL, to which either Bthba (7.5 μmol, 4.2 mg) or COF-TpBth powder (3.5 mg) was added, and the mixture was reacted at 25 °C for 8 minutes. For the shredded COF membrane, the reactants included an ethanol solution of benzaldehyde (0.5 M, 0.25 mmol, 26.5 mg) and malononitrile (0.55 M, 0.275 mmol, 18.2 mg) in a total volume of 0.15 mL, also reacted at 25 °C for 8 minutes. The reaction yield was determined via ^{1}H NMR spectroscopy.

Membrane catalysis in the condensation of benzaldehyde and ethyl cyanoacetate. The catalytic setup is the same as that used in the condensation of benzaldehyde and malononitrile. 0.5 mL ethanol

solution containing ethyl cyanoacetate (0.55 M) and benzaldehyde (0.5 M) was introduced into the feed chamber at 25 °C and 0.05 bar of vacuum suction was applied. The yield of the membrane catalysis was determined using ^{1}H NMR spectroscopy.

Batch reactions in the condensation of benzaldehyde and ethyl cyanoacetate. The volumes of the reaction solutions for batch reactions were determined based on the flux through the membrane. For example, in the COF-TpBth/PES membrane reactor operating at a temperature of 25 °C and under a vacuum suction of 0.05 bar, 0.15 mL of solution passed through within 8 minutes. The quantities of COF powders and homogeneous catalysts used were calculated based on the mass of the COF active layers. To aid in the weighing process, the batch reactions were scaled up by a factor of 100. The reaction mixture consisted of an ethanol solution with benzaldehyde (0.5 M, 7.5 mmol, 795.9 mg) and ethyl cyanoacetate (0.55 M, 8.25 mmol, 848.3 mg), totaling 15 mL, to which either Bthba (7.5 μmol, 4.2 mg) or COF-TpBth powder (3.5 mg) was added, and the mixture was reacted at 25 °C for 8 minutes. The reaction yield was determined via ^{1}H NMR spectroscopy.

Membrane catalysis in the ring-opening reaction between styrene oxide and ethanol. The catalytic setup is the same as that used in the condensation of benzaldehyde and malononitrile. 0.5 mL ethanol solution containing styrene oxide (0.5 M) was introduced into the feed chamber at 35 °C and 0.05 bar of vacuum suction was applied. The yield of the membrane catalysis was determined using ^{1}H NMR spectroscopy.

Batch reactions in the ring-opening reaction between styrene oxide and ethanol. The volumes of the reaction solutions for batch reactions were determined based on the flux through the membrane. For example, in the COF-TpBth/PES membrane reactor operating at a temperature of 35 °C and under a vacuum suction of 0.05 bar, 0.15 mL of solution passed through within 8 minutes. The quantities of COF powders and homogeneous catalysts used were calculated based on the mass of the COF active layers. To aid in the weighing process, the batch reactions were scaled up by a factor of 100. The reaction mixture consisted of an ethanol solution with styrene oxide (0.5 M, 7.5 mmol, 795.9 mg), totaling 15 mL, to which either Bthba (7.5 μmol, 4.2 mg) or COF-TpBth powder (3.5 mg) was added, and the mixture was reacted at 35 °C for 8 minutes. The reaction yield was determined via ^{1}H NMR spectroscopy.

Data availability

The authors declare that all the data supporting the findings of this study are available within the article (and Supplementary Information files), or available from the corresponding author on request.

References

1. Vankelecom, I. F. J. Polymeric membranes in catalytic reactors. *Chem. Rev.* **102**, 3779–3810 (2002).
2. Thyssen, V. V., Vilela, V. B., de Florio, D. Z., Ferlauto, A. S. & Fonseca, F. C. Direct conversion of methane to C_2 hydrocarbons in solid-state membrane reactors at high temperatures. *Chem. Rev.* **122**, 3966–3995 (2022).
3. Li, X. et al. Efficient flow synthesis of aspirin within 2D sub-nanoconfined laminar annealed graphene oxide membranes. *Adv. Mater.* **36**, 2310954 (2024).
4. Luo, Y. et al. Efficient electrocatalytic N_2 fixation with MXene under ambient conditions. *Joule* **3**, 279–289 (2019).
5. Ye, L., Li, H. & Xie, K. Sustainable ammonia production enabled by membrane reactor. *Nat. Sustain.* **5**, 787–794 (2022).
6. Zhu, X. & Yang, W. Microstructural and interfacial designs of oxygen-permeable membranes for oxygen separation and reaction-separation coupling. *Adv. Mater.* **31**, 1902547 (2019).
7. Didaskalou, C. et al. Membrane-grafted asymmetric organocatalyst for an integrated synthesis-separation platform. *ACS Catal* **8**, 7430–7438 (2018).
8. Fischer, L., Volz, A., Hagemann, U. & Ulbricht, M. Polymeric multi-composites with a tailored nickel microenvironment as catalytic flow-through membrane reactors for efficient *p*-nitrophenol degradation. *Chem. Eng. J.* **463**, 142437 (2023).
9. Tran, N. N. et al. Enzymatic pretreatment of recycled grease trap waste in batch and continuous-flow reactors for biodiesel production. *Chem. Eng. J.* **426**, 131703 (2021).
10. Yue, W. et al. Highly selective CO_2 conversion to methanol in a bifunctional zeolite catalytic membrane reactor. *Angew. Chem. Int. Ed.* **60**, 18289–18294 (2021).
11. Li, H. et al. Na^+-gated water-conducting nanochannels for boosting CO_2 conversion to liquid fuels. *Science* **367**, 667–671 (2020).
12. Zeng, G. et al. Dual-role membrane as NH_3 permselective reactor and azeotrope separator in urea alcoholysis. *ACS Cent. Sci.* **5**, 1834–1843 (2019).
13. Sakbodin, M. et al. Direct nonoxidative methane conversion in an autothermal hydrogen-permeable membrane reactor. *Adv. Energy Mater.* **11**, 2102782 (2021).
14. Diercks, C. S. & Yaghi, O. M. The Atom, the molecule, and the covalent organic framework. *Science* **355**, eaal1585 (2017).
15. Geng, K. et al. Covalent organic frameworks: design, synthesis, and functions. *Chem. Rev.* **120**, 8814–8933 (2020).
16. Colson, J. W. & William, R. D. Rationally synthesized two-dimensional polymers. *Nat. Chem.* **5**, 453–465 (2013).
17. Kandambeth, S., Dey, K. & Banerjee, R. Covalent organic frameworks: chemistry beyond the structure. *J. Am. Chem. Soc.* **141**, 1807–1822 (2019).
18. Lohse, M. S. & Bein, T. Covalent organic frameworks: structures, synthesis, and applications. *Adv. Funct. Mater.* **28**, 1705553 (2018).
19. Li, Y. et al. De novo design and facile synthesis of 2D covalent organic frameworks: a two-in-one strategy. *J. Am. Chem. Soc.* **141**, 13822–13828 (2019).
20. Guan, X. et al. Chemically stable polyarylether-based covalent organic frameworks. *Nat. Chem.* **11**, 587–594 (2019).
21. Liu, Y. et al. Vinylene-linked 2D conjugated covalent organic frameworks by Wittig reactions. *Angew. Chem. Int. Ed.* **61**, e202209762 (2022).
22. Xie, Y. et al. Tuning the topology of three-dimensional covalent organic frameworks via steric control: from pts to unprecedented ljh. *J. Am. Chem. Soc.* **143**, 7279–7284 (2021).
23. Banerjee, T. et al. Single-site photocatalytic H_2 evolution from covalent organic frameworks with molecular cobaloxime Co-catalysts. *J. Am. Chem. Soc.* **139**, 16228–16234 (2017).
24. Ma, T. et al. Single-crystal X-ray diffraction structures of covalent organic frameworks. *Science* **361**, 48–52 (2018).
25. Yang, J. et al. Advancing osmotic power generation by covalent organic framework monolayer. *Nat. Nanotechnol.* **17**, 622–628 (2022).
26. Ding, S.-Y. et al. Construction of covalent organic framework for catalysis: Pd/COF-LZU1 in Suzuki Miyaura coupling reaction. *J. Am. Chem. Soc.* **133**, 19816–19822 (2011).
27. Zhao, X., Pachfule, P. & Thomas, A. Covalent organic frameworks (COFs) for electrochemical applications. *Chem. Soc. Rev.* **50**, 6871–6913 (2021).
28. Yuan, C. et al. Mixed-linker chiral 2D covalent organic frameworks with controlled layer stacking for electrochemical asymmetric catalysis. *J. Am. Chem. Soc.* **146**, 635–645 (2024).

29. Zhu, H.-J. et al. Oxygen-tolerant CO_2 electroreduction over covalent organic frameworks via photoswitching control oxygen passivation strategy. *Nat. Commun.* **15**, 1479 (2024).
30. Basak, A., Karak, S. & Banerjee, R. Covalent organic frameworks as porous pigments for photocatalytic metal-free C–H borylation. *J. Am. Chem. Soc.* **145**, 7592–7599 (2023).
31. Zhao, W. et al. Accelerated synthesis and discovery of covalent organic framework photocatalysts for hydrogen peroxide production. *J. Am. Chem. Soc.* **144**, 9902–9909 (2022).
32. Haug, W. K., Wolfson, E. R., Morman, B. T., Thomas, C. M. & McGrier, P. L. A nickel-doped dehydrobenzoannulene-based two-dimensional covalent organic framework for the reductive cleavage of inert aryl C–S bonds. *J. Am. Chem. Soc.* **142**, 5521–5525 (2022).
33. You, P.-Y. et al. Reversible modulation of interlayer stacking in 2D copper-organic frameworks for tailoring porosity and photocatalytic activity. *Nat. Commun.* **15**, 194 (2024).
34. Lu, S. et al. Synthesis of ultrafine and highly dispersed metal nanoparticles confined in a thioether-containing covalent organic framework and their catalytic applications. *J. Am. Chem. Soc.* **139**, 17082–17088 (2017).
35. Xu, H., Gao, J. & Jiang, D. Stable, crystalline, porous, covalent organic frameworks as a platform for chiral organocatalysts. *Nat. Chem.* **7**, 905–912 (2015).
36. Gong, Y.-N. et al. Regulating photocatalysis by spin-state manipulation of cobalt in covalent organic frameworks. *J. Am. Chem. Soc.* **142**, 16723–16731 (2020).
37. Zhu, H.-J. et al. Efficient electron transmission in covalent organic framework nanosheets for highly active electrocatalytic carbon dioxide reduction. *Nat. Commun.* **11**, 497 (2020).
38. Fan, Y., Kang, D. W., Labalme, S. & Lin, W. A spirobifluorene-based covalent organic framework for dual photoredox and nickel catalysis. *J. Am. Chem. Soc.* **145**, 25074–25079 (2023).
39. Sun, Q. et al. Pore environment control and enhanced performance of enzymes infiltrated in covalent organic frameworks. *J. Am. Chem. Soc.* **140**, 984–992 (2018).
40. López-Magano, A. et al. Recent advances in the use of covalent organic frameworks as heterogenous photocatalysts in organic synthesis. *Adv. Mater.* **35**, 2209475 (2023).
41. Romero-Muñiz, I. et al. Unveiling the local structure of palladium loaded into imine-linked layered covalent organic frameworks for cross-coupling catalysis. *Angew. Chem. Int. Ed.* **59**, 13013–13020 (2020).
42. Sheng, F. et al. Efficient ion sieving in covalent organic framework membranes with sub-2-nanometer channels. *Adv. Mater.* **33**, 2104404 (2021).
43. Cao, L. et al. Giant osmotic energy conversion through vertical-aligned ion-permselective nanochannels in covalent organic framework membranes. *J. Am. Chem. Soc.* **144**, 12400–12409 (2022).
44. Xin, W. et al. Tunable molecular transport and sieving enabled by covalent organic framework with programmable surface charge. *Mater. Today* **51**, 56–64 (2021).
45. Wang, M. et al. Ultrafast seawater desalination with covalent organic framework membranes. *Nat. Sustain.* **5**, 518–526 (2022).
46. Wang, K. et al. Monolayer-assisted surface-initiated Schiff-base-mediated aldol polycondensation for the synthesis of crystalline sp^2 carbon-conjugated covalent organic framework thin films. *J. Am. Chem. Soc.* **145**, 5203–5210 (2023).
47. Meng, Q.-W. et al. Guanidinium-based covalent organic framework membrane for single-acid recovery. *Sci. Adv.* **9**, eadh0207 (2023).
48. Guo, Q. et al. Photoelectric responsive ionic channel for sustainable energy harvesting. *Nat. Commun.* **14**, 6702 (2023).
49. Halder, A. et al. Interlayer hydrogen-bonded covalent organic frameworks as high-performance supercapacitors. *J. Am. Chem. Soc.* **140**, 10941–10945 (2018).
50. Knebel, A. & Caro, J. Metal-organic frameworks and covalent organic frameworks as disruptive membrane materials for energy-efficient gas separation. *Nat. Nanotechnol.* **17**, 911–923 (2022).
51. Shi, X. et al. Design of three-dimensional covalent organic framework membranes for fast and robust organic solvent nanofiltration. *Angew. Chem. Int. Ed.* **61**, e202207559 (2022).
52. Zhao, S. et al. Hydrophilicity gradient in covalent organic frameworks for membrane distillation. *Nat. Mater.* **20**, 1551–1558 (2021).
53. Yang, H., Xu, J., Cao, H., Wu, J. & Zhao, D. Recovery of homogeneous photocatalysts by covalent organic framework membranes. *Nat. Commun.* **14**, 2726 (2023).
54. Li, J. et al. Ultramicroporous covalent organic framework nanosheets with functionality pair for membrane C_2H_2/C_2H_4 separation. *Angew. Chem. Int. Ed.* **62**, e202216675 (2023).
55. List, B. Emil Knoevenagel and the roots of aminocatalysis. *Angew. Chem. Int. Ed.* **49**, 1730–1734 (2010).
56. Kong, Y. et al. Manipulation of cationic group density in covalent organic framework membranes for efficient anion transport. *J. Am. Chem. Soc.* **145**, 27984–27992 (2023).
57. Bing, W. et al. A CaMnAl-hydrotalcite solid basic catalyst toward the aldol condensation reaction with a comparable level to liquid alkali catalysts. *Green Chem.* **20**, 3071–3080 (2018).
58. Zhang, X., Liu, H. & Jiang, L. Wettability and applications of nanochannels. *Adv. Mater.* **31**, 1804508 (2019).
59. Nazari, M., Davoodabadi, A., Huang, D., Luo, T. & Ghasemi, H. Transport phenomena in nano/molecular confinements. *ACS Nano* **14**, 16348–16391 (2020).
60. Thomas, J. A. & McGaughey, A. J. H. Reassessing fast water transport through carbon nanotubes. *Nano Lett.* **8**, 2788–2793 (2008).
61. Zhang, X., Lai, E. S. M., Martin-Aranda, R. & Yeung, K. L. An investigation of Knoevenagel condensation reaction in microreactors using a new zeolite catalyst. *Appl. Catal. A: Gen.* **261**, 109–118 (2004).
62. Yang, Y. et al. Structure-induced Lewis-base $Ga_4B_2O_9$ and its superior performance in Knoevenagel condensation reaction. *Mol. Catal.* **490**, 110914 (2020).
63. Ball, P. Water as an active constituent in cell biology. *Chem. Rev.* **108**, 74–108 (2008).
64. Park, H. G. & Jung, Y. Carbon nanofluidics of rapid water transport for energy applications. *Chem. Soc. Rev.* **43**, 565–576 (2014).

Acknowledgements

This research received funding from the National Key Research and Development Program of China (Grant Nos. 2022YFA1503004 to Q.S. and X.M.), the National Science Foundation of China (Grant No. 22205198 to S.W.), and the Zhejiang Provincial Natural Science Foundation of China (Grant Nos. LR23B060001 and LY23B060022 to Q.S. and S.W., respectively). We appreciate the assistance of Fang Chen from Analytical Testing Center of the Department of Chemistry, Zhejiang University, in conducting SEM measurements.

Author contributions

Q.S. and Z.D. conceived and designed the research. L.Z. conducted the membrane synthesis and the majority of the testing. Z.Z. performed the MD simulation. Z.L., S.Y., W.X., and Q.W.M. contributed to the membrane characterization. Y.X., X.M., S.M., and F.S.X. provided valuable suggestions. All authors contributed to drafting the paper and approved the final version of the manuscript.

Competing interests

The authors declare no competing interests.

Additional information

Supplementary information The online version contains supplementary material available at https://doi.org/10.1038/s41467-024-51250-8.

Correspondence and requests for materials should be addressed to Zhifeng Dai or Qi Sun.

Peer review information *Nature Communications* thanks the anonymous, reviewer(s) for their contribution to the peer review of this work. A peer review file is available.